JOURNAL OF IMAGING SCIENCE AND TECHNOLOGY • Volume 41, Number 2, March/April 1997

Drying of Water-Based Inks on Plain Paper*

M. Sami Selim, Victor F. Yesavage, Rachid Chebbi, and Seung H. Sung
Colorado School of Mines, Golden, Colorado 80401

Jens Borch and John M. Olson†
Lexmark International, Boulder, Colorado 80301

Previous studies in ink-jet printing have considered ink penetration into paper or ink evaporation to be effective in the drying process. In the present study, a unified approach that allows for simultaneous evaporation and penetration during the drying process was applied. To this end, penetration rates were measured experimentally using a Bristow tester. In addition, evaporation rates were determined from a theoretical evaporation model that contained no adjustable parameters. It was found that for plain paper used in the office environment, the rate of penetration was at least 20 × higher than the rate of evaporation. Accordingly, ink drying is determined mainly by penetration, and penetration curves alone are sufficient to predict the dry time or ink disappearance on a plain paper surface. In practice, this is illustrated by ink-jet print quality on plain papers of various sizing treatments. The sizing level needs to be adjusted according to the desired ink-jet image. That is, full-color printing requires penetration rates sufficient to accommodate each of the process inks applied without color bleed or other ink-to-ink interaction processes. This may be at expense of character and line print deterioration due to fiber swelling in mono-color printing.

Journal of Imaging Science and Technology 152–158 (1997)

Introduction

In spite of recent advances in ink-jet paper manufacture[1] spurred by the rapid growth in low-end color printers, a detailed understanding of the ink drying process is still lacking. This is particularly so for the plain paper types used in the office environment. Generally, these are treated with chemicals that provide water resistance to the paper (sizing treatments). While this is beneficial to the general end usage of these papers, it also may provide a tremendous variation in print quality for ink-jet printing depending on ink formulation and printer design. The complexity of the paper structure, both physically and chemically, provides several ways in which a water-based ink may penetrate.[2] For ink-jet drops impacting the paper surface at relatively high speeds, analysis has been restricted to mainly visual observation of dried drop sizes[3] or quantitative measurements using video analysis.[2] For larger liquid volumes, quantitative penetration measurements can be carried out more readily, using, for example, the Bristow test procedure.[4] The Bristow tester is a useful tool for comparing the liquid uptake of different plain papers but, so far, it has not been shown to simulate the ink-jet printing process for the much smaller ink drop volumes. Most studies in ink-jet printing have emphasized the ink penetration into paper as being the main mechanism for drying without considering the additional effect of ink evaporation. In contrast, one study[5] has treated ink evaporation as the main controlling drying step. Another study[2] has considered evaporation as being too slow to contribute to the drying process. In the present approach simultaneous evaporation and penetration will be considered. Penetration measurements will be based on Bristow test analysis.

Theory

Our goal is to develop a mathematical model that can be used to predict the drying rate of a water-based ink film deposited on a paper surface. To this end, we first develop an evaporation model that can be applied to calculate the rate of drying under the assumption that drying takes place due to evaporation alone. The model, which is free from any adjustable parameters, is developed for a pure liquid evaporating in a quiescent atmosphere under isothermal conditions. Evaporation rates calculated from this model provide the maximum evaporation rate possible for a water-based ink film under quiescent conditions. Next, we present a model that can be used to calculate the penetration rate of ink into paper. The penetration model is based on the Lucas-Washburn equation that requires knowledge of the absorption coefficient. The latter can be determined experimentally; for example, using a Bristow tester. Finally, we use results from both models to arrive at a combined model that allows for ink drying under simultaneous evaporation and penetration into the paper.

Evaporation Model. Consider a water-based ink film of initial height Z_0 and initial temperature T_∞ as shown in Fig. 1. Water evaporates from the flat ink surface into a vapor region that extends an infinite distance above the ink surface. The vapor consists of the diffusant A (water vapor) and a gas B (air) that is insoluble in the liquid film. The initial concentration of A, ρ_{A0}, and the initial temperature, T_∞, in the gas phase are both uniform. At any time t, the ink film occupies the region $0 < z < Z(t)$ and the air occupies the region $Z(t) < z < \infty$, where $Z(t)$ denotes the position of the evaporating interface. The desire is to find an expression for the location of the ink–air interface $Z(t)$ as a function of time t.

Original manuscript received October 16, 1996.

† IS&T Member

* Presented in part at the 46th Annual Conference of IS&T, the Society for Imaging Science and Technology, Cambridge, MA, May 9-14, 1993 and at the 47th Annual Conference of IS&T, Rochester, NY, May 15-20, 1994.

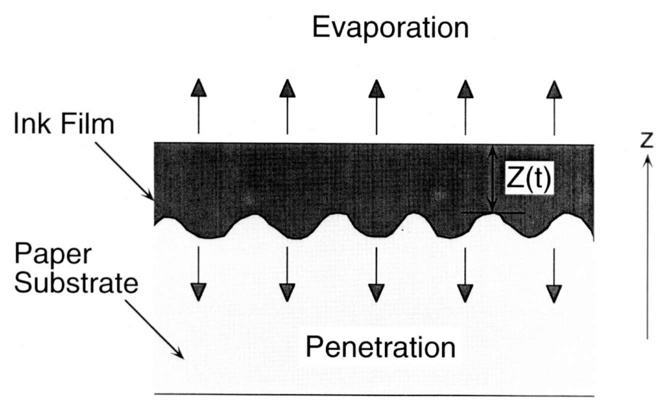

Figure 1. Water-based ink film evaporating from and penetrating into a paper substrate.

To seek an analytical solution to the problem, we assume an ink film consisting of pure liquid water and neglect any temperature variation during the evaporation process. Thus, we consider the evaporation of a pure liquid under isothermal conditions. Under these conditions, the solution will provide an upper bound for the evaporation rate of a water-based ink on paper. This is because the lowering of the liquid temperature due to evaporation or the addition of glycol to the ink will result in a lowering of the water vapor pressure at the ink–air interface and hence the evaporation rate.

With these assumptions, the process will be controlled by mass diffusion of the evaporating species (water vapor) through the vapor phase. Accordingly, the appropriate equations governing the mass concentration, ρ_A, of the water vapor through the vapor region may be written as:

$$\frac{\partial \rho_A}{\partial t} + \left(1 - \frac{\rho_L}{\rho_v}\right) \frac{dZ}{dt} \frac{\partial \rho_A}{\partial z} = D_{AB} \frac{\partial^2 \rho_A}{\partial t^2}, \quad Z(t) < z < \infty, \tag{1}$$

subject to the following initial and boundary conditions:

$$Z = Z_0, \qquad t = 0, \tag{2}$$

$$\rho_A = \rho_{A0}, \qquad Z_0 < z < \infty, t = 0, \tag{3}$$

$$\rho_A = \rho_{A,eq}, \qquad Z = Z(t), t > 0, \tag{4}$$

$$D_{AB} \frac{\partial \rho_A}{\partial z} = \rho_L \left(1 - \frac{\rho_{A,eq}}{\rho_v}\right) \frac{dZ}{dt}, \quad Z = Z(t), t > 0, \tag{5}$$

$$\rho_A = \rho_{A0}, \qquad Z \to \infty, t > 0. \tag{6}$$

In Eq. 1, ρ_V denotes the mass density of the vapor phase, ρ_L denotes the mass density of the liquid phase, and D_{AB} is the diffusion coefficient of A in B. The quantity $\rho_{A,eq}$ in Eqs. 4 and 5 represents the gas-phase concentration of A at the moving interface. For the case of isothermal evaporation of a pure liquid, $\rho_{A,eq}$ is constant.

Equations 1 through 6 are readily solved using similarity transformations with the similarity variable $\eta = 2\sqrt{D_{AB}t}$. The final solution is given by

$$\frac{\rho_A - \rho_{A0}}{\rho_{A,eq} - \rho_{A0}} = \frac{\operatorname{erfc}\left\{\frac{z - Z_0}{\sqrt{4D_{AB}t}} - \left(1 - \frac{\rho_L}{\rho_v}\right)\lambda\right\}}{\operatorname{erfc}\left(\frac{\rho_L}{\rho_v}\lambda\right)}, \tag{7}$$

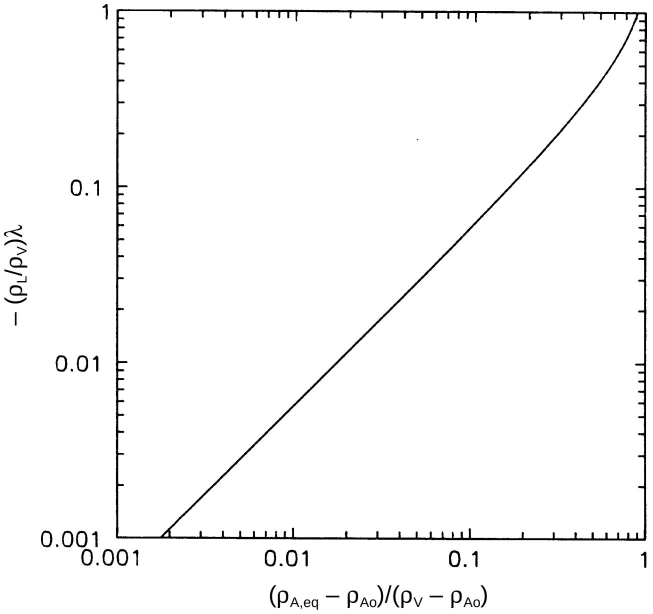

Figure 2. Graph based on Eq. 10 for determining the evaporation parameter λ.

$$Z(t) = Z_0 + 2\lambda\sqrt{D_{AB}t}, \tag{8}$$

$$\frac{dZ}{dt} = \lambda\sqrt{\frac{D_{AB}}{t}}, \tag{9}$$

where λ is the root of the following transcendental equation:

$$\left(\frac{\rho_L}{\rho_v}\lambda\right) \operatorname{erfc}\left(\frac{\rho_L}{\rho_v}\lambda\right) \exp\left(\frac{\rho_L}{\rho_v}\lambda\right)^2 = -\frac{1}{\sqrt{\pi}} \frac{\rho_{A,eq} - \rho_{A0}}{\rho_v - \rho_{A,eq}}. \tag{10}$$

Equation 7 gives the concentration distribution of water vapor in the gas phase as a function of z and t, Eq. 8 gives the location of the evaporation front as a function of time, and Eq. 9 gives the velocity of the evaporation front. The root λ of Eq. 10 may be interpreted as the dimensionless location of the evaporation front, $[Z(t) - Z_0]/\sqrt{4D_{AB}t}$, and also as the dimensionless evaporation front velocity, $(dZ/dt)/\sqrt{D_{AB}t}$. The solution of Eq. 10 for λ is readily determined using the Newton-Raphson method[6] and is presented in Fig. 2. Note that the abscissa in this figure is not the group appearing on the right of Eq. 10. The abscissa in this figure is a more convenient group in practice and is related to the group on the right side of Eq. 10 as follows:

$$\frac{\rho_{A,eq} - \rho_{A0}}{\rho_V - \rho_{A,eq}} = \frac{\dfrac{\rho_{A,eq} - \rho_{A0}}{\rho_V - \rho_{A0}}}{1 - \dfrac{\rho_{A,eq} - \rho_{A0}}{\rho_V - \rho_{A0}}}. \tag{11}$$

Using regression analysis, numerical results from the solution of Eq. 10 were used to develop the following explicit equations for λ:

$$\ln \lambda^* = -0.5247 + 1.0091 \ln \rho^*, \quad \text{for } 0.001 < \rho^* < 0.1, \tag{12}$$

$$\ln \lambda^* = 0.1771 + 2.1679 \ln \rho^* + 0.7016[\ln \rho^*]^2 + 0.1449[\ln \rho^*]^3, \quad \text{for } 0.1 < \rho^* < 1.0, \tag{13}$$

where

$$\lambda^* = -\frac{\rho_L}{\rho_V}\lambda \quad \text{and} \quad \rho^* = \frac{\rho_{A,eq} - \rho_{A0}}{\rho_V - \rho_{A0}}. \tag{14}$$

For a water-based ink evaporating under TAPPI conditions of 23°C and 50% RH, we find $\rho_V = 1.194$ kg/m^3, $\rho_L = 1000$ kg/m^3, $\rho_{A0} = 0.01027$ kg/m^3, and $\rho_{A,eq} = 0.02054$ kg/m^3. With these values, Eq. 12 gives

$$\lambda = -5.86 \times 10^{-6} \tag{15}$$

Taking the diffusivity of water vapor in air at 23°C as 2.6×10^4 μ^2/ms, Eq. 9 gives the evaporation rate as

$$\left(\frac{dZ}{dt}\right)_{\text{evap}} = -\frac{9.45 \times 10^{-4}}{\sqrt{t}}\ \mu\text{m / ms}. \tag{16}$$

The minus sign in this equation indicates that $Z(t)$ decreases with time. Note that the z axis is taken positive in the upward direction.

Penetration Model. The penetration of an ink film into paper is readily obtained from the Lucas-Washburn equation[7] if a hydrophobic liquid is applied. For more hydrophilic liquids, such as water-based ink films, the penetration mode is more complex.[8,9] Penetration may be faster due to fiber swelling and capillary expansion or slower due to saturation of liquid into capillaries.[9,10] Additionally, the process is affected by the specific interaction between the liquid and the surface chemistry of the paper fibers in the surface structure.[11] Based on this and Bristow penetration analysis of water penetration into paper structures including plain printing papers,[9] we propose to use the following equation for the penetration rate of an ink film into paper:

$$V = K_r + K_a(t^m - t_w^m)ml / m^2, \tag{17}$$

where V is the volume of liquid absorbed into the paper in ml/m^2, t is the time in ms, K_r is the roughness index in ml/m^2, and K_a is the absorption coefficient in ml/(m$^2\cdot$ms^m). Because a thickness of 1 μm is equivalent to a volume of 1 ml/m^2, Eq. 17 also may be written as

$$Z(t) = K_r + K_a(t^m - t_w^m)\mu m, \tag{18}$$

where K_r is now in μm and K_a in μm/ms^m. Note that the numerical values of K_r and K_a are identical.

Differentiating Eq. 18 with respect to time, we obtain the penetration rate as:

$$\left(\frac{dZ}{dt}\right)_{\text{pent}} = -mK_a t^{m-1}\mu\text{m / ms}. \tag{19}$$

Note that a minus sign has been inserted on the right side of Eq. 19 because the film thickness decreases with time as penetration occurs.

Combined Evaporation and Penetration Model. We now consider ink film drying by evaporation and penetration. Because both processes occur simultaneously, a mass balance on the ink film gives

$$\left(\frac{dZ}{dt}\right) = \left(\frac{dZ}{dt}\right)_{\text{evap}} + \left(\frac{dZ}{dt}\right)_{\text{pent}}. \tag{20}$$

Substituting for the evaporation and penetration rates from Eqs. 9 and 19, we obtain

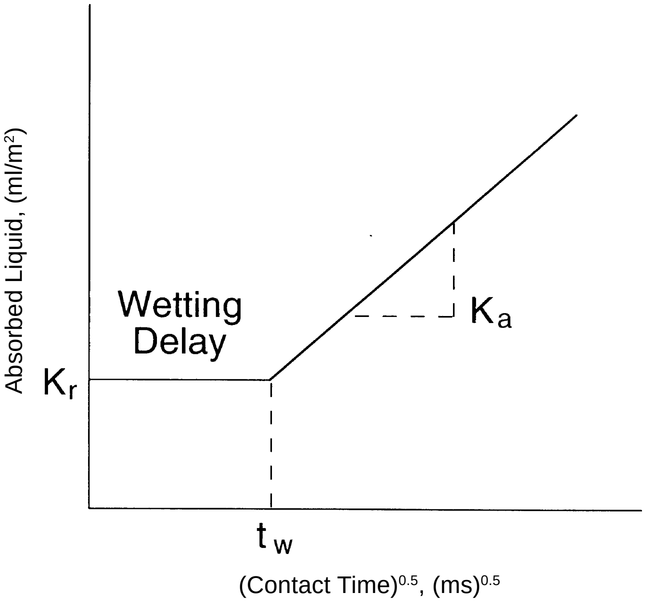

Figure 3. Bristow plot describing the liquid uptake versus square root of time.

$$\left(\frac{dZ}{dt}\right) = \lambda\sqrt{\frac{D_{AB}}{t}} - mK_a t^{m-1}. \tag{21}$$

Integration of this equation gives the following expression for the variation of the film thickness with time:

$$Z(t) = Z_0 + 2\lambda\sqrt{D_{AB}t} - K_a t^m. \tag{22}$$

For the values of λ and D_{AB} given above, Eqs. 21 and 22 become

$$\left(\frac{dZ}{dt}\right) = -\frac{9.45 \times 10^{-4}}{\sqrt{t}} - mK_a t^{m-1}\mu m / ms, \tag{23}$$

$$Z(t) = Z_0 - 0.0019\sqrt{t} - K_a t^m \mu\text{m}. \tag{24}$$

Experimental

Using Eq. 23 for the ink film thickness decrease or Eq. 24 for the ink film thickness at different times requires the measurement of K_a and m via plots like that shown in Fig. 3 where $m = 0.5$. Using mixtures of ethylene glycol and water, this was carried out for two copy paper brands; one typical of the acid-made rosin-sized paper used for xerographic copying and laser printing and the other typical of the alkaline-made synthetic-sized paper now being substituted for the acid-made paper grade in mill conversions.[12] Figures 4 and 5 show the liquid volume uptake variations on a square-root time basis ($m = 0.5$). For the rosin-sized paper (Fig. 4), K_a varied from 0.11 to 0.27 depending on the ethylene glycol content. For the synthetic-sized paper (Fig. 5), liquid uptake was much more rapid and could not be measured for ethylene glycol concentrations higher than 20% because of complete penetration of the relatively thin (≈100 μm) 20-lb paper base. Additionally, it is apparent that square-root time linearity is not followed for the synthetic-sized paper brand. The liquid uptake on a square-root time basis is not linear but may be brought to a linear basis by assuming a higher exponent of time ($m = 0.9$) as shown in Fig. 6. In this case K_a varied from 0.025 to 0.044.

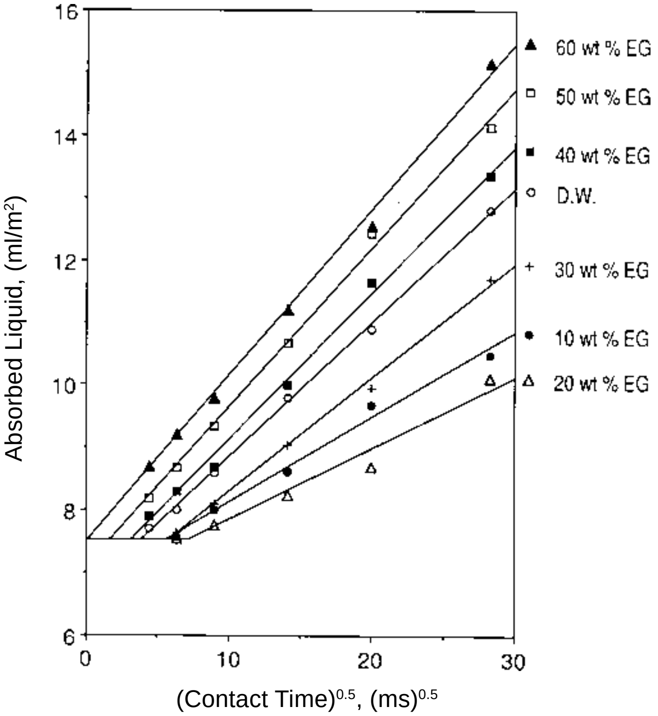

Figure 4. Liquid uptake versus square root of time for rosin-sized paper.

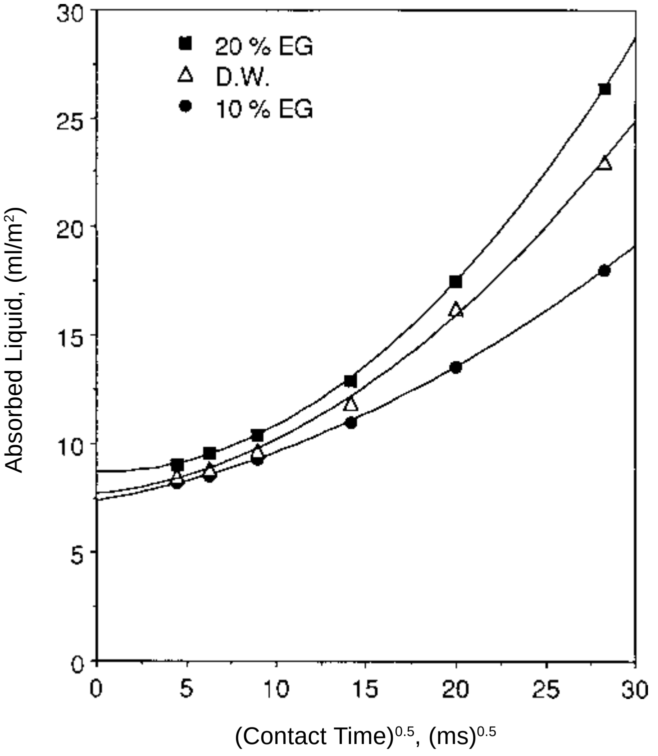

Figure 5. Liquid uptake versus square root of time for synthetic-sized paper.

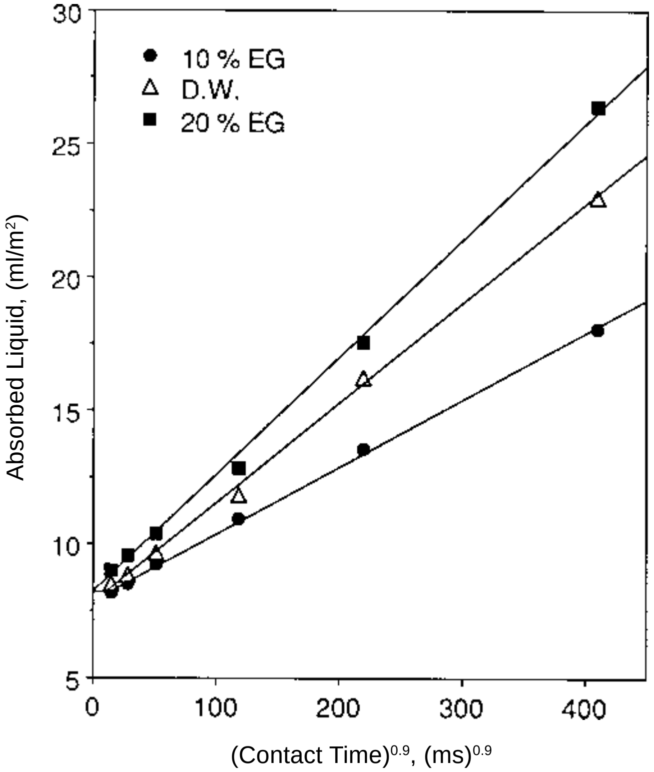

Figure 6. Liquid uptake for synthetic-sized paper on linear basis (m = 0.9).

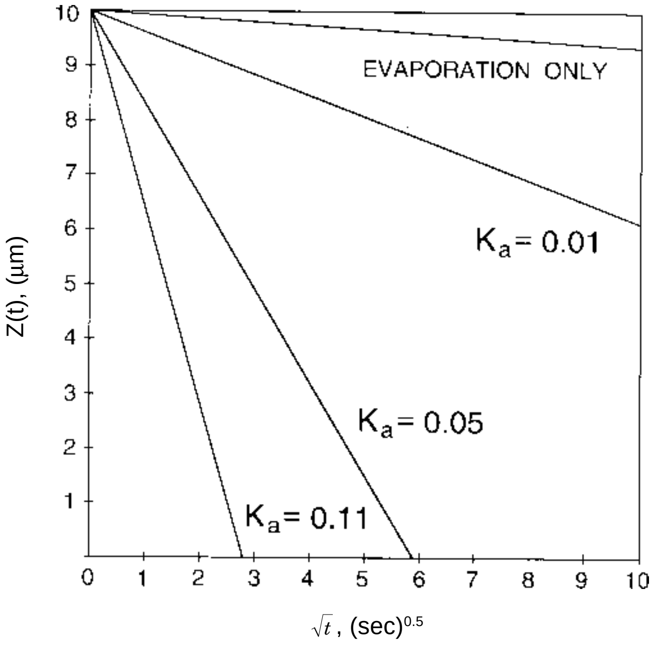

Figure 7. Calculated film thickness variation with time for a 10-μm-thick film drying by evaporation alone and by penetration with absorption coefficients K_a = 0.01, 0.05, and 0.11.

Results

Evaporation versus Penetration. For m = 0.5 in Eq. 24 and the K_a values found for the rosin-sized paper (the least penetrating paper), it is apparent that the film thickness loss due to evaporation is of the order of 1% of that due to penetration. Lower values for K_a have been reported in the literature,[13] but still at these levels, the thickness loss due to penetration is about 20 times larger than the corresponding loss due to evaporation. Lower penetration rates are possible for papers by adding more sizing (hard-sized papers), changing the chemical nature of the sizing, or varying the filler or paper structure. However, this creates drying rates that are unacceptably high for ink-jet printing. This is seen from calculated results presented in

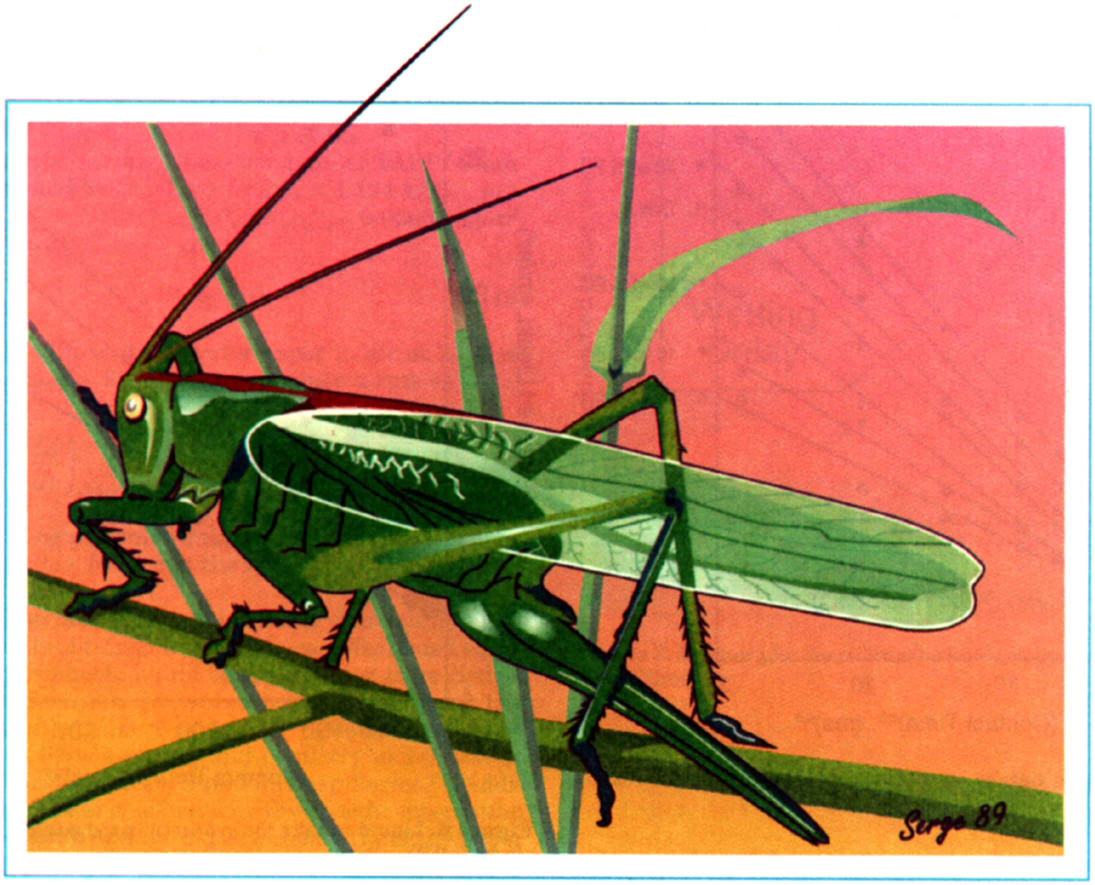

Figure 8. Color reproduction of full-color print quality on paper similar to that tested in Fig. 4.

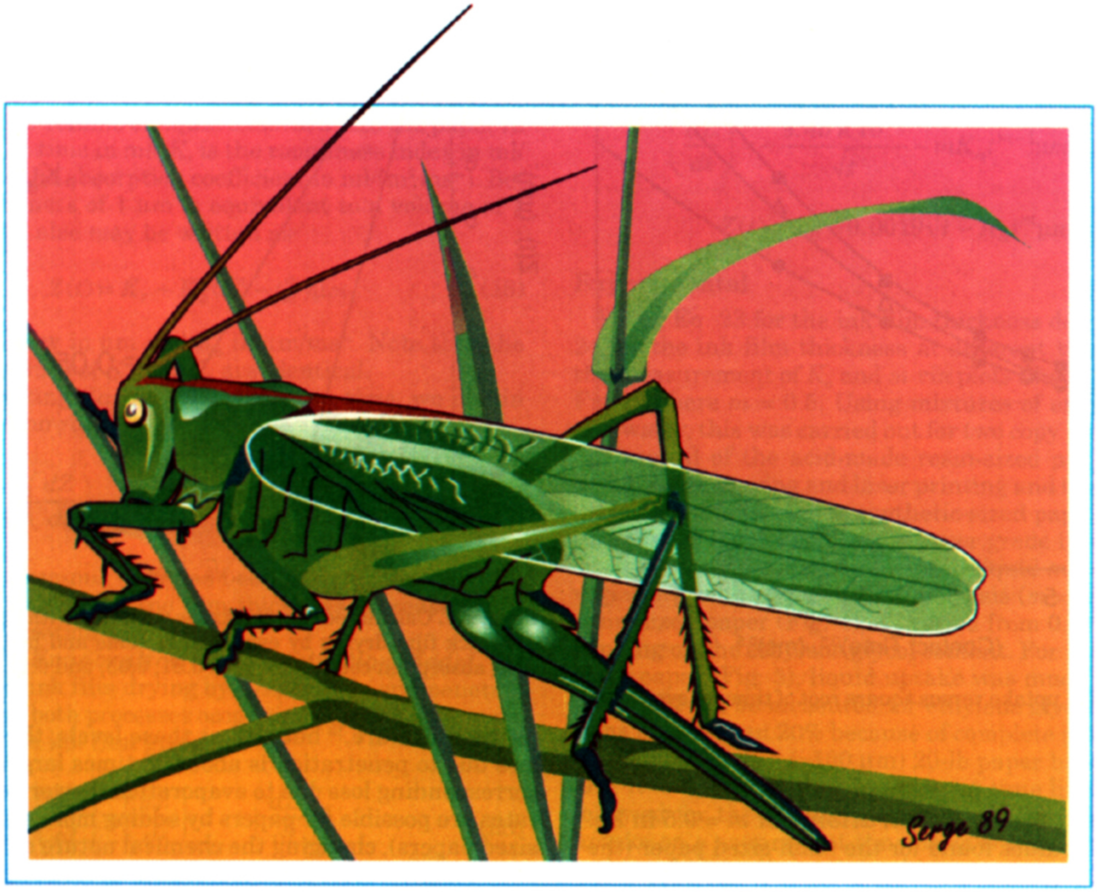

Figure 9. Color reproduction of full-color print quality on paper similar to that tested in Figs. 5 and 6.

Fig. 7, where the film loss due to drying of a 10-μm-thick film is compared to drying at different penetration levels and to drying due to evaporation alone. For K_a levels below 0.11, the drying time increases beyond 10 s. The even slower drying by evaporation alone agrees with the experimental findings of Oliver, Agbezuge, and Woodcock,[2] for drying of ink-jet drops on nonpenetrating mylar material. For evaporation to play a role in ink-jet drying one must increase the proportionality factor defined by λ beyond the value (0.0019) given in Eq. 24. This can be done through ink formulation (nonwater-based inks) or by heat assistance. Several ink-jet printers have been marketed relying on the latter principle.

Discussion

Print Quality. To test the results obtained using the modeling approach and Bristow testing with glycol water mixtures, full-color printing was carried out on various copy papers using an IBM Color Jetprinter PS 4079.* This printer prints with composite inks of relatively low glycol content (≈20%) at a relatively high speed requiring rapid ink drying. All printing was carried out under *TAPPI* environmental conditions (*TAPPI* T402) such that evaporation rates should be very similar for all of the papers tested and similar to that assumed in the theoretical calculation. Yet, print quality varied greatly as seen in Fig. 8 for an acid-made rosin-sized paper similar to the one quantified by Bristow testing and in Fig. 9 for one like the alkaline-made synthetic-sized paper also studied by Bristow testing. The rosin-sized paper exhibited graininess due to color bleed in full-color areas but superior character and line definition for single-color printing. The synthetic-sized sheet showed much better print definition in full-color areas but at the expense of more raggedness for character and line printing. We believe that this behavior simulates the penetration characteristics defined by Bristow testing. The higher penetration rate for the synthetic-sized sheet results in drying the ink amounts applied in full-color printing by transferring individual colors from the sheet surface before another is applied. The lower penetration rate for the rosin-sized sheet creates a situation where colors bleed together before drying. Because differences in evaporation rates were not created, the difference in print quality must be solely due to penetration. The deterioration in character and line printing for slack-sized paper is well known for lower resolution black-on-white ink-jet printers.[3,14] For the 4079 printer, this difference is less pronounced but becomes visible in single-dot printing as shown in Figs. 10 and 11. Dot fuzziness in the alkaline-made paper (Fig. 11) may be interpreted as created by ink penetration into fiber cell walls and lumens immediately after ink-paper contact as indicated by the instant upward curvature of the Bristow plot in Fig. 5.[9,10] Dot definition is much less dependent on fiber structure in the acid-made paper (Fig. 10). This is due to wetting delay followed by nonswelling penetration (Fig. 4). Here, Bristow testing appears to simulate aspects of ink-jet printing in that sufficient paper sizing prevents penetration into the fiber structure. Note that the paper acidity depends mainly on the filler used and not so much on paper fiber structure or sizing and also that paper acidity by itself is not the major variable in determining print quality.

Conclusions

- By comparing evaporation rates calculated using an experimental model with penetration rates obtained using Bristow testing, we conclude that drying rates depend on paper penetration in ink-jet printing with water-based inks.

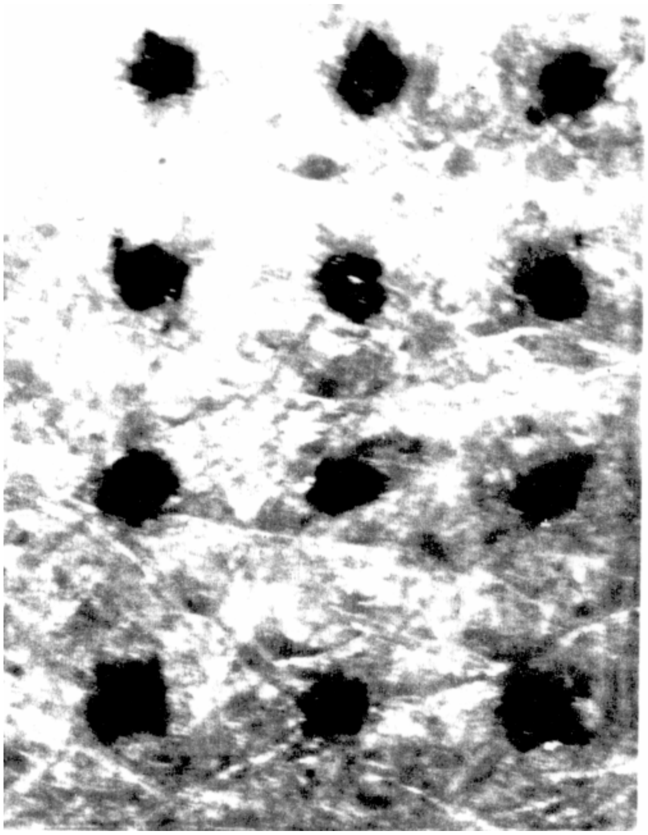

Figure 10. Single-dot images on paper similar to that tested in Fig. 4.

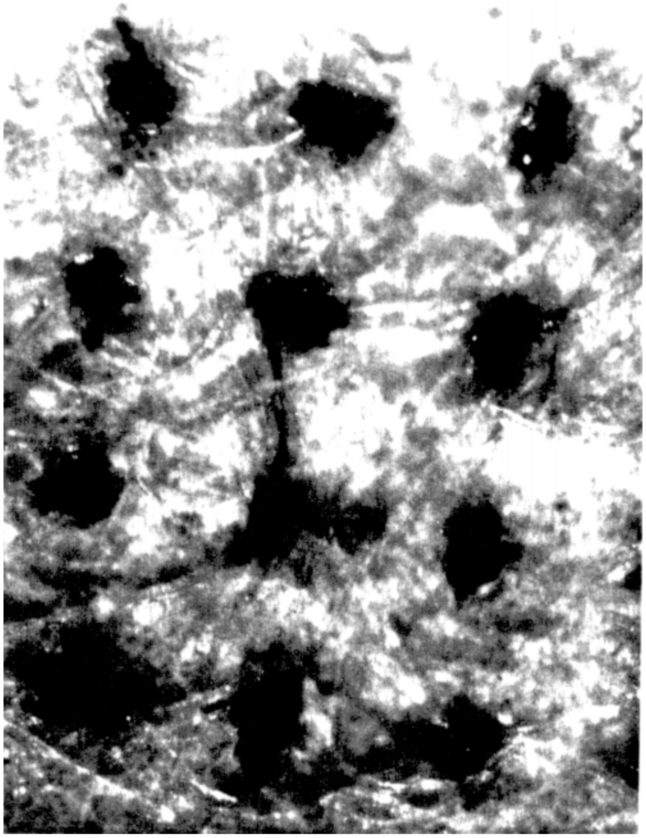

Figure 11. Single-dot images on paper similar to that tested in Figs. 5 and 6.

- Because penetration is the functional process in non-heat-assisted ink-jet printing, paper sizing contributes to ink-jet image on plain paper brands. That is, full-color printing requires penetration rates sufficient to accommodate each of the process inks applied without color bleed or other ink-to-ink interaction processes. However, this may be at the expense of character and line print deterioration due to fiber swelling in mono-color printing.

* IBM is a registered trademark and Color Jetprinter is a trademark of International Business Machines Corporation in the United States and/ or other countries and used under license.

References

1. D. L. Lee, W. H. Fass, and A.T. Winslow, *Advance Printing of Papers, IS&T's 47th Annual Conference/ICPS 1994,* Rochester, NY, 823 (1994).
2. J. F. Oliver, L. Agbezuge, and K. Woodcock, *Proceedings of IS&T's 7th International Congress on Advances in Non-Impact Printing Technologies,* Portland, OR, 163 (1991).
3. S. J. Bares, in *Handbook of Imaging Materials,* A. S. Diamond, Ed., Marcel Dekker, Inc., New York, 1991, pp. 545–562.
4. ASTM Standard D 5455-93.
5. A. Borhan, S. B. Pence, and A. H. Sporer, *J. Imaging Technol.* **16:** 65 (1990).
6. W.S. Dorn and D.D. McCracken, *Numerical Methods*, John Wiley & Sons, Inc., New York, 1972, pp. 25–30.
7. M. B. Lyne, in *Handbook of Physical and Mechanical Testing of Paper and Paperboard,* **2**, R. E. Mark, Ed., Marcel Dekker, Inc., New York, 1984, pp. 103–141.
8. R. W. Hoyland, in *Fiber–Water Interactions in Paper-Making,* F. Bolam, Ed., British Paper and Board Federation, London, 1978, pp. 557–577.
9. M. B. Lyne and J. S. Aspler, *Tappi* **65:** 98 (1982).
10. M. B. Lyne, in *Products of Papermaking,* **2***,* C. F. Baker, Ed., Pira International, Leatherhead, U.K., 1993, pp. 885–911.
11. J. Borch, in *Products of Papermaking,* **1***,* C. F. Baker, Ed., Pira International, Leatherhead, U.K., 1993, pp. 209–236.
12. J. Borch, *TAPPI Short Course Notes, 1990 Neutral/Alkaline Papermaking Short Course,* Orlando, FL, 39 (1990).
13. M. Shimomura, Y. Sato, Y. Suga, and H. Noguchi, *J. Imaging Technol.* **16:** 189 (1990).
14. S. J. Bares and K. R. Rennels, *Tappi J.* **73:** 123 (1990).